This article has been accepted for inclusion in a future issue of this journal. Content is final as presented, with the exception of pagination.

Two-Terminal and Multi-Terminal Designs for Next-Generation Quantized Hall Resistance Standards: Contact Material and Geometry

Mattias Kruskopf, Albert F. Rigosi, Alireza R. Panna, Dinesh K. Patel, Hanbyul Jin, Martina Marzano, Michael Berilla, David B. Newell, and Randolph E. Elmquist, *Senior Member, IEEE*

***Abstract*— In this paper, we show that quantum Hall resistance measurements using two terminals may be as precise as four-terminal measurements when applying superconducting split contacts. The described sample designs eliminate resistance contributions of terminals and contacts such that the size and complexity of next-generation quantized Hall resistance devices can be significantly improved.**

***Index Terms*— Epitaxial graphene (EG), multi-series (MS) contacts, quantum Hall effect (QHE), quantized Hall resistance (QHR) standards, superconducting contacts.**

I. Introduction

QUANTUM effects in epitaxial graphene (EG) devices allow for robust quantum Hall effect (QHE) resistance plateaus at $R_H = R_K/2 = h/2e^2$, where R_H is the Hall resistance, and R_K is the von Klitzing constant [1]–[3]. By using series and parallel connections as building blocks, we can construct quantum Hall array resistance standards (QHARS) that provide multiple quantized resistance values [4]–[9]. However, resistance networks based on multiple quantized Hall resistance (QHR) devices often suffer from accumulated resistances at contacts and interconnections. In this paper, we show that quantized resistances, normally measured at four terminals for high precision, can also be measured at two terminals by eliminating undesired resistances when applying superconducting split contacts. While multi-series (MS) interconnections of QHE devices have been extensively studied and applied for the construction of QHARS, we show that the principle can also be applied to improve the performance of contacts of single QHR elements significantly. Together with using superconducting materials, these improvements open new routes in the design of next-generation resistance standards.

II. Device Preparation and Characterization

The device fabrication process, as shown in Fig. 1(a), is based on the technique of protecting the EG from lithographic residues with a thin Pd/Au layer to allow for contaminant-free graphene/metal contacts [10], [11]. The covered EG is then structured into the Hall bar geometry using a thicker Au metal masking layer and Ar plasma etching. The ≈320-nm-thick superconducting NbTiN layer for the contacts and contact pads is sputtered onto a ≈7.5-nm-thin Ti adhesion layer and is then covered by ≈30 nm Pt to prevent surface oxidation. In the last step, photolithography is applied to open a window to the Pd/Au covered EG which is then wet-etched using diluted aqua regia. The wet-etching procedure removes the Pd/Au in the defined areas without harming the EG. The finished devices are functionalized with chromium tricarbonyl [$Cr(CO)_3$], which provides tunable and uniform doping without the need for large-scale electrostatic gates [12].

To assess the superconducting behavior of the contacts, the resistance of a finished device was monitored as a function of temperature with a lock-in amplifier system. As shown in Fig. 1(b), two points shorted by a NbTiN element exhibit a discontinuous reduction in the four-wire resistance after falling below the critical temperature (T_c) of about 12.5 K at zero magnetic field. Using a nanovoltmeter and a current-reversal measurement technique to eliminate thermal voltages, the resistance at 1.6 K was determined to be zero ($-0.31 \pm 3.63\ \mu\Omega$) within the measurement uncertainty. At $B = 9$ T, the critical temperature was reduced by about 2 K and is still far above the typical measurement temperature of ≤ 4.2 K.

Fig. 1(c) shows a confocal laser scanning microscope (CLSM) image of a graphene device source/drain (S/D) region with superconducting split contacts with six branches. Labels indicate the high and low equipotential edges, separated by hot spots that appear in the quantum Hall regime and mark the points where dissipation occurs [13], [14]. Depending on

Manuscript received April 24, 2019; revised June 12, 2019; accepted June 26, 2019. The review of this paper was arranged by Editor C. Yang. *(Corresponding author: Mattias Kruskopf.)*

M. Kruskopf and H. Jin are with the Department of Physics, Joint Quantum Institute, University of Maryland, College Park, MD 20742 USA, and also with the National Institute of Standards and Technology (NIST), Gaithersburg, MD 20899 USA (e-mail: mattias.kruskopf@nist.gov; hanbyul.jin@nist.gov).

A. F. Rigosi, A. R. Panna, M. Berilla, D. B. Newell, and R. E. Elmquist are with the National Institute of Standards and Technology, Gaithersburg, MD 20899 USA (e-mail: albert.rigosi@nist.gov; alireza.panna@nist.gov; michael.berilla@nist.gov; david.newell@nist.gov; randolph.elmquist@nist.gov).

D. K. Patel is with the Graduate Institute of Applied Physics, National Taiwan University, Taipei 10617, Taiwan (e-mail: dkpjnp@gmail.com).

M. Marzano is with the Politecnico di Turin, Istituto Nazionale di Ricerca Metrologica, 10135 Turin, Italy (e-mail: m.marzano@inrim.it).

Color versions of one or more of the figures in this paper are available online at http://ieeexplore.ieee.org.

Digital Object Identifier 10.1109/TED.2019.2926684

This article has been accepted for inclusion in a future issue of this journal. Content is final as presented, with the exception of pagination.

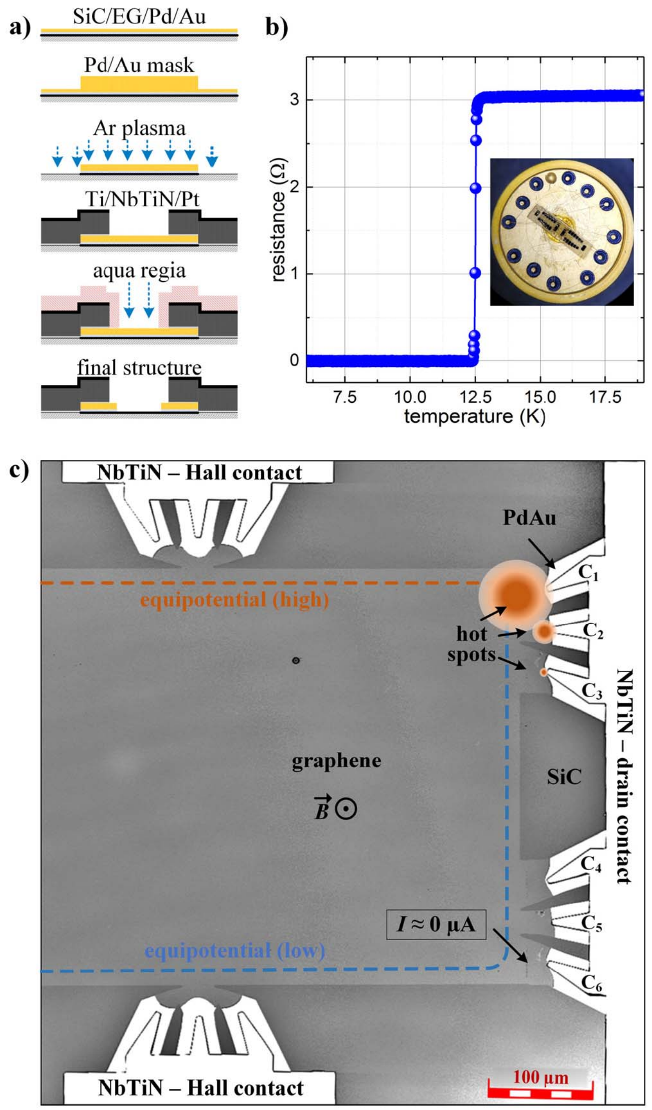

Fig. 1. (a) Photolithography process for graphene device fabrication using superconducting NbTiN contacts is divided into six steps (from the top to the bottom). (b) Resistance measurements of the superconducting NbTiN contacts show vanishing resistance below the critical transition temperature $T_c \approx 12.5$ K. The inset represents the top-view onto the sample with two devices mounted onto a TO-8 header. (c) CLSM image of a graphene Hall device shows the structured graphene (light gray structure) as well as the drain contact (right) and two Hall contacts (top and bottom). By splitting each contact into multiple individual branches, the resulting contact resistance becomes negligible in the quantum Hall regime. The drawn hot spots at the contacts indicate that most of the current enters the first branch (C_1) of the contact while the current is reduced by $\varepsilon/2$. The current in the last branch $I_{C6} \approx 0$ μA describes equilibrium between the electric potential of the contacts and the QHE edge channels as well as an approximately zero contact S/D resistance.

the direction of the applied magnetic field, the hot-spots occur in different corners of the device. For interconnected S/D contact points separated by more than an inelastic scattering length, most of the current enters via the very first branch (C_1), closest to the corner [15]. Thus, for MS QHE devices, the current in each of the following branches denoted by $C_2, \ldots, C_n$ of a split contact is progressively lower by factors of $\varepsilon/2 = (R_{\text{branch}}/R_H)/2$ [4]. In the case of three or more distinct branches with individual contact resistances on the order of $R_{\text{branch}} = 1$–10 Ω, the current in the last branch (C_n) becomes negligible, and thus the overall contact resistance is negligible.

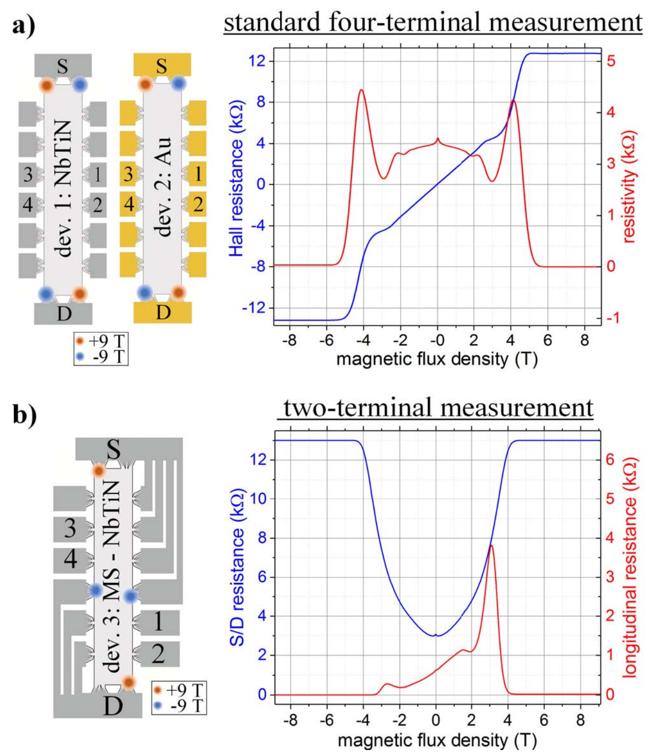

Fig. 2. (a) Device 1 (NbTiN contacts) and device 2 (Au contacts) represent typical devices for standard four-terminal/four-contact QHR measurements. The corresponding magnetic field sweep of device 1 shows the behavior of the Hall resistance with a linear slope at low fields (2 T $> B >$ −2 T) and QHR plateaus of the converse sign at high fields above ±5.5 T. The hot spots for the opposite magnetic field direction are shown in red. The longitudinal resistivity is highly symmetric in both field directions. (b) Device 3 (MS-NbTiN) uses MS connection for two-terminal measurements to eliminate contributions of the longitudinal resistance when operating at +9T. The magnetic field dependence of the resistance in the two-terminal configuration across the source/drain (S/D) contacts shows a symmetrical, nonlinear behavior at low fields up to $B = \pm 4.5$ T and extended resistance plateaus at high fields of $|B| \geq 5$ T). The longitudinal resistance shows an asymmetrical behavior depending on the direction of the magnetic field due to significant changes in the current path. The expected positions of the hot spots in the quantum Hall regime are indicated by the red and blue marked locations for positive and negative magnetic flux densities. The numbers and labels of the contacts describe the ones that were used for the measurements as given in the legends.

III. Results and Discussion

To test the performance of the split contacts, three different processes/designs for making device contacts were tested. The left side of Fig. 2(a) shows that device 1 (NbTiN) and device 2 (Au) use the same design but a different main contact material component. The corresponding measurement for device 1 on the right of Fig. 2(a) shows the typical magnetic field dependence in the standard four-terminal resistance measurement configuration of EG-based QHE devices. At the measurement temperature of 1.6 K, the charge carrier density and mobility were $n = 1.33 \times 10^{11}$ cm^{-2} and $\mu = 15040$ cm^2/Vs, respectively.

Device 3, as shown on the left in Fig. 2(b), has MS connections at the high and low potential sides of the Hall bar.

This design provides an optimum measurement configuration for one magnetic field direction, where hot spots are shown in blue because the influence of remnant longitudinal resistivity is minimized as with an ideal four-terminal configuration. The resistance across the S/D contacts in the two-terminal/MS configuration, as shown on the right side of Fig. 2(b), is symmetric in the two field directions, with an extended resistance plateau starting around $B = \pm 5$ T. The high dependence of the longitudinal resistance on the B-field direction, as shown in Fig. 2(b), is due to the asymmetric current path for positive and negative field directions at low fields. The changing positions of the hot spots when going from $B = +9$' T to $B = -9$ T are indicated by the blue and red spots, respectively.

The precision measurements in Fig. 3(a) were performed using a direct current comparator (DCC) resistance bridge [16] for device 1 (NbTiN) and a binary cryogenic current comparator (BCCC) bridge [17] for device 2 (Au) and device 3 (MS-NbTiN). We determined the resistance value in the two-terminal configuration using four wires (blue triangles) and the standard four-terminal configuration (red stars). The pin configuration can be understood from the numbers and labels given in the legend of the measurements and the drawings of the devices in Fig. 2. The deviation from the nominal QHR value is calculated from $\delta = (R - R_K/2)/R$, where R is the measured Hall resistance. In the four-terminal measurement configuration, the deviation from nominal was -1.4 ± 21 nΩ/Ω for device 1 and 5.3 ± 9.8 nΩ/Ω for device 2. In the two-terminal configuration, the deviation was 19 ± 17 nΩ/Ω, 620 ± 7.9 nΩ/Ω and 12 ± 3.5 nΩ/Ω for devices 1, 2, and 3, respectively. The uncertainties show the type A uncertainties ($k = 1$). Under the assumption of perfect quantization, implying a negligible contribution of the longitudinal resistance in the two-terminal resistance measurement, we can estimate the S/D contact resistance R_{cont} from the difference $\Delta = R - (R_K/2)$ where $R_{\text{cont}} = \Delta/2$ [18]. The resulting contact resistances are $124 \pm 110\ \mu\Omega$, $4029 \pm 51\ \mu\Omega$ and $77 \pm 22\ \mu\Omega$ for devices 1, 2, and 3, respectively. Under the more realistic assumption of a nonzero longitudinal resistivity of about $10\ \mu\Omega$, the contact resistances of devices 1 and 2 are even lower. A typical longitudinal resistance across the whole length of the device would be about $55\ \mu\Omega$ considering the dimensions of the Hall bar ($400\ \mu$m $\times$ $2200\ \mu$m).

Fig. 3(b) shows longitudinal resistance data from the low equipotential side of the three devices taken using an analog nanovoltmeter, with direct current (dc) reversal to eliminate thermal voltages. The red stars show standard longitudinal resistance measurements in the four-terminal configuration by measuring the voltage between two neighboring Hall contacts 3 and 4. The blue triangles describe the resistance across the Hall contact 3 and the drain contact in a three-terminal configuration. Any significant difference in the two is expected to be due to the voltage drop at the drain contact. The results of the devices 1 and 3 using superconducting split contacts are consistent with the measurements shown in Fig. 3(a) and support the understanding that the contact resistance and the longitudinal resistance are both, indeed, close to zero within the measurement uncertainty. A clear deviation from zero $580 \pm 260\ \mu\Omega$ was observed when measuring across

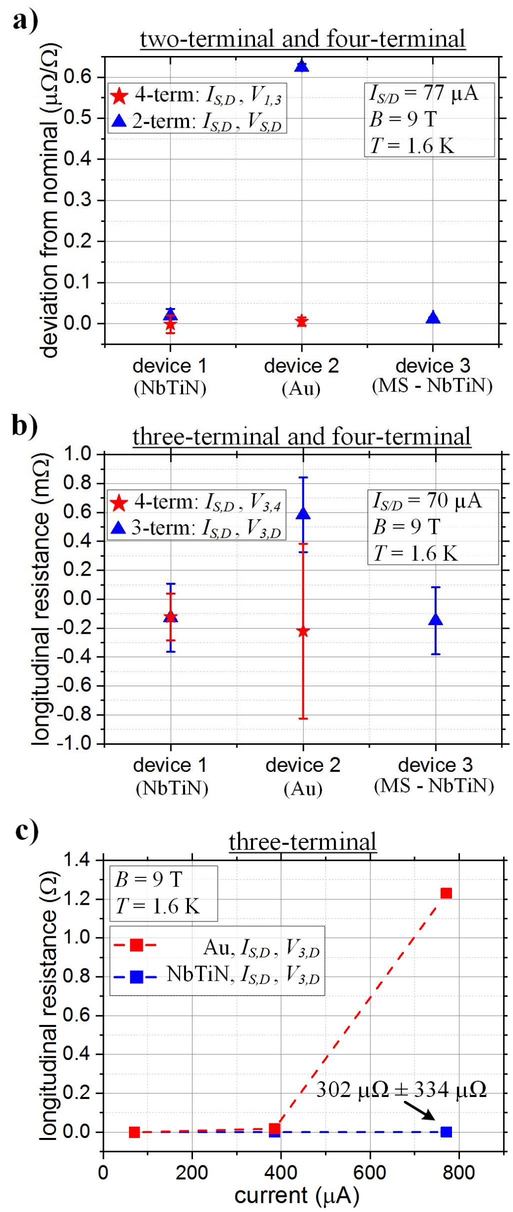

Fig. 3. (a) Precision QHR measurements using cryogenic current comparator (CCC) and DCC measurement systems show the deviation of the measured resistance from the nominal value of $R_K/2 = h/2e^2 \approx 12906.4\ \Omega$. Device 1 (NbTiN) and device 2 (Au) were measured in the standard four-terminal (4-term, red stars) and two-terminal (2-term, blue triangles) measurement configuration while device 3 (MS NbTiN) was measured in the two-terminal configuration only. The labeling of the pins used for the measurements given in the legend corresponds to the labels given in Fig. 2. In the two-terminal configuration, the deviation from nominal is on the order of 10 nΩ/Ω when using NbTiN contacts and approximately 600 nΩ/Ω in the case of Au contacts. In the standard four-terminal configuration, the deviation from nominal is 0 nΩ/Ω within the measurement uncertainty. The error bars indicate the type A uncertainty ($k = 1$) of the measurements. (b) Longitudinal measurements at the low potential side of the Hall bar were performed applying dc current reversal and using a nanovoltmeter. The longitudinal resistances were determined by measuring the voltage drop between neighboring Hall contacts using four terminals (4-term, red stars) as well as between a Hall contact and the drain contact using three terminals (3-term, blue triangles). The vanishing three-terminal longitudinal resistance across the drain contact indicates exceptionally small effective contact resistances in the case of device 1 (NbTiN) and device 3 (MS-NbTiN). The error bars indicate the standard deviation of the measurements. (c) In contrast to Au contacts (device 2, red square), three-terminal longitudinal resistance measurements between the Hall and drain contact show no significant current dependence at currents as high as 771 μA in the case of NbTiN contacts (device 1, blue square).

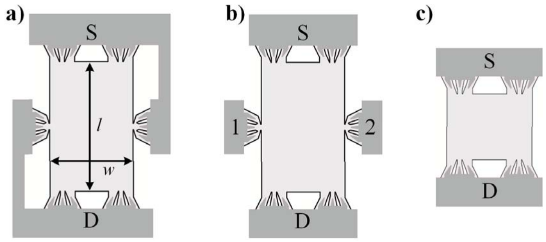

Fig. 4. (a) This element combines the principle of superconducting split contacts and a double series connection. Since the Hall voltage is defined in the center of the device, no longitudinal resistance component is added to the measurement. When deployed in QHARS networks, this element allows for miniaturized designs and simplified processing by eliminating the need for multilayer lithography processes. (b) Removing the series connection allows for two-terminal as well as standard four-terminal measurements. (c) Removing the Hall contacts results in the most compact and simplest design. Such elements with reduced complexity may be beneficial for ac-QHR measurements due to potentially reduced capacitive losses. An appropriate width to length ratio of the QHR channel for the designs given in (a)–(c) is suggested to be w/l = 1/2, w/l = 1/2 and w/l = 1, respectively.

the Au Hall and drain contact of device 2. The slightly lower value compared to the one determined from the measurement in Fig. 3(a) suggests that sample inhomogeneities have led to higher longitudinal resistances in some parts of this device. Since Ti/Au contacts of graphene quantum Hall devices reported in the literature have typically yielded contact resistances of 1 Ω or higher [19], this paper reports on the order of 10^4 times lower resistances compared to most previously reported values.

Fig. 3(c) shows further investigations of the longitudinal resistance and contact resistance behavior using three terminals at high currents of device 1 (NbTiN, blue data points) and device 2 (Au, red data points). The data shows a strong increase in the resistance when measuring between the Hall contact 3 and the drain contact in the case of device 2. In the case of device 1, the resistance was surprisingly unaffected with a near-zero value of $302 \pm 334\ \mu\Omega$ when applying the highest current of 771 μA.

State-of-the-art series-connected QHR elements require complicated lithography steps to realize multi-layer interconnections and to ensure that the Hall contacts have no electrical contact to the S/D contacts while crossing the current path [6], [20]. This is to avoid picking up any Hall voltages occurring in the S/D metal contact pads as well as voltages due to the S/D current and ohmic resistance in the region of the current terminals. The realization of QHE devices with vanishing contact resistances and no additional dissipation at interconnections provided using superconducting materials allows for significant simplifications in the design of future quantized resistance standards. In Fig. 4, three miniaturized QHE elements are proposed that may be used in resistance metrology as individual devices or as the smallest cell for the construction of QHARS.

The element shown in Fig. 4(a) is designed to provide a quantized resistance value that is free of longitudinal resistance contributions since the Hall voltage is defined in the center of the two sides. It is especially suitable for the construction of series-connected elements in arrays because of its optimized two-terminal design. It sacrifices the additional contact used to measure the value of the longitudinal resistance to minimize the size. Using a superconductor instead of normal metallic interconnections eliminates undesired contributions at these interconnections such that voltage and current terminals can be the same. Note that the superconductor must have a critical temperature and a critical field significantly above the measurement conditions to avoid the occurrence of nonzero Hall fluctuations [21], [22].

As demonstrated by the results of devices 1 and 2 shown in Fig. 3, superconducting split contacts allow for precise measurements in the two-terminal and the four-terminal definition. The design shown in Fig. 4(b) condenses the multi-terminal Hall bar design to the minimum number of contacts while maintaining access to both Hall and longitudinal measurements. Note that when performing longitudinal measurements between the low-potential Hall contact and drain, the result is always a sum of the contact resistance and the longitudinal resistance in the edge channels [18]. Fig. 4(c) shows the smallest possible QHARS element and may only be used in the two-terminal configuration, like the design shown in Fig. 4(a). Even though longitudinal resistance in the 2-D region may affect the value of the QHR in this design, the smaller square design reduces both the channel length and the resulting longitudinal resistance by a factor of two. For highly uniform EG, the introduced error is expected to be small enough to allow for measurements with a deviation from nominal on the order of 10 nΩ/Ω or less. The reduction in complexity and size would also help to minimize capacitive losses at alternating current and might allow for ac-QHE measurements with improved precision compared to formerly used designs [23], [24].

IV. Conclusion

While normally measured at four terminals for high precision, in this paper, we demonstrate that the QHR can be precisely measured at two terminals by employing split-contacts. The reason why branched contacts allow for voltage and resistance measurements that are unaltered by contact resistances is the current injection into the 2-D electron gas at the hot spots in the quantum Hall regime. Since the contact resistance is defined by the interfaces at this spot, the resistance cannot be reduced by increasing the length of the contact. Only additional branches allow the formation of additional hot spots that are much smaller and compensate the voltage drop across previous branches such that the potential equilibrium between the 2DEG and the contact is reached. Additionally, the application of superconducting materials eliminates undesired ohmic resistances and Hall voltages in the terminals. The elimination of resistance contributions of terminals and contacts enables new avenues of device design for future resistance standards using crossover-free series and parallel connected elements and will help to minimize capacitive losses at alternating currents for impedance standards. As shown in this paper, the principle of combining superconductivity and optimized contact design has a great potential to improve the performance of single QHR standards and QHARS devices.

Acknowledgment

The work of D. K. Patel at NIST was made possible by arrangement with C.-T. Liang of National Taiwan University, and the work of M. Marzano at NIST was made possible by arrangement with M. Ortolano of Polytechnic University of Turin and L. Callegaro of the Istituto Nazionale di Ricerca Metrologica, Turin, Italy.

References

[1] K. V. Klitzing and G. Ebert, "Application of the quantum Hall effect in metrology," *Metrologia*, vol. 21, no. 1, pp. 11–18, Jan. 1985. doi: 10.1088/0026-1394/21/1/004.

[2] K. S. Novoselov *et al.*, "Two-dimensional gas of massless dirac Fermions in graphene," *Nature*, vol. 438, no. 7065, pp. 197–200, Nov. 2005. doi: 10.1038/nature04233.

[3] T. J. B. M. Janssen *et al.*, "Precision comparison of the quantum Hall effect in graphene and gallium arsenide," *Metrologia*, vol. 49, no. 3, pp. 294–306, Mar. 2012. doi: 10.1088/0026-1394/49/3/294.

[4] F. Delahaye, "Series and parallel connection of multiterminal quantum Hall-effect devices," *J. Appl. Phys.*, vol. 73, no. 11, pp. 7914–7920, Feb. 1993. doi: 10.1063/1.353944.

[5] W. Poirier, A. Bounouh, F. Piquemal, and J. P. André, "A new generation of QHARS: Discussion about the technical criteria for quantization," *Metrologia*, vol. 41, no. 4, pp. 285–294, Jun. 2004. doi: 10.1088/0026-1394/41/4/010.

[6] T. Oe, S. Gorwadkar, T. Itatani, and N.-H. Kaneko, "Development of 1 MΩ quantum Hall array resistance standards," *IEEE Trans. Instrum. Meas.*, vol. 66, no. 6, pp. 1475–1481, Jun. 2017. doi: 10.1109/TIM.2016.2620218.

[7] A. Lartsev, S. Lara-Avila, A. Danilov, S. Kubatkin, A. Tzalenchuk, and R. Yakimova, "A prototype of RK/200 quantum Hall array resistance standard on epitaxial graphene," *J. Appl. Phys.*, vol. 118, no. 4, Jul. 2015, Art. no. 044506. doi: 10.1063/1.4927618.

[8] M. Ortolano, M. Abrate, and L. Callegaro, "On the synthesis of quantum Hall array resistance standards," *Metrologia*, vol. 52, no. 1, pp. 31–39, Dec. 2014. doi: 10.1088/0026-1394/52/1/31.

[9] S. Novikov *et al.*, "Mini array of quantum Hall devices based on epitaxial graphene," *J. Appl. Phys.*, vol. 119, no. 17, May 2016, Art. no. 174504. doi: 10.1063/1.4948675.

[10] M. Kruskopf and R. E. Elmquist, "Epitaxial graphene for quantum resistance metrology," *Metrologia*, vol. 55, no. 4, pp. R27–R36, Aug. 2018. doi: 10.1088/1681-7575/aacd23.

[11] Y. Yang *et al.*, "Epitaxial graphene homogeneity and quantum Hall effect in millimeter-scale devices," *Carbon*, vol. 115, pp. 229–236, May 2017. doi: 10.1016/j.carbon.2016.12.087.

[12] A. F. Rigosi *et al.*, "Gateless and reversible carrier density tunability in epitaxial graphene devices functionalized with chromium tricarbonyl," *Carbon*, vol. 142, pp. 468–474, Feb. 2019. doi: 10.1016/j.carbon.2018.10.085.

[13] J. Weis and K. von Klitzing, "Metrology and microscopic picture of the integer quantum Hall effect," *Philos. Trans. Roy. Soc. A, Math. Phys. Eng. Sci.*, vol. 369, no. 1953, pp. 3954–3974, Oct. 2011. doi: 10.1098/rsta.2011.0198.

[14] K. Ikushima, H. Sakuma, S. Komiyama, and K. Hirakawa, "Visualization of quantum Hall edge channels through imaging of terahertz emission," *Phys. Rev. B, Condens. Matter*, vol. 76, no. 16, Oct. 2007, Art. no. 165323. doi: 10.1103/PhysRevB.76.165323.

[15] M. Büttiker, "Absence of backscattering in the quantum Hall effect in multiprobe conductors," *Phys. Rev. B, Condens. Matter*, vol. 38, no. 14, pp. 9375–9389, Nov. 1988. doi: 10.1103/PhysRevB.38.9375.

[16] M. P. MacMartin and N. L. Kusters, "A direct-current-comparator ratio bridge for four-terminal resistance measurements," *IEEE Trans. Instrum. Meas.*, vol. 15, no. 4, pp. 212–220, Dec. 1966. doi: 10.1109/TIM.1966.4313542.

[17] M. Götz and D. Drung, "Stability and performance of the binary compensation unit for cryogenic current comparator bridges," *IEEE Trans. Instrum. Meas.*, vol. 66, no. 6, pp. 1467–1474, Jun. 2017. doi: 10.1109/TIM.2017.2659998.

[18] G. L. J. A. Rikken *et al.*, "Two-terminal resistance of quantum Hall devices," *Phys. Rev. B, Condens. Matter*, vol. 37, no. 11, pp. 6181–6186, Apr. 1988. doi: 10.1103/PhysRevB.37.6181.

[19] T. Yager *et al.*, "Low contact resistance in epitaxial graphene devices for quantum metrology," *AIP Adv.*, vol. 5, no. 8, Aug. 2015, Art. no. 087134. doi: 10.1063/1.4928653.

[20] J. Könemann, C. Leicht, F.-J. Ahlers, E. Pesel, K. Pierz, and H. W. Schumacher, "Investigation of Serial Quantum Hall arrays as a Quantum Resistance Standard," *J. Phys. Conf. Ser.*, vol. 334, no. 1, Dec. 2011, Art. no. 012017. doi: 10.1088/1742-6596/334/1/012017.

[21] N. P. Breznay and A. Kapitulnik, "Observation of the ghost critical field for superconducting fluctuations in a disordered TaN thin film," *Phys. Rev. B, Condens. Matter*, vol. 88, no. 10, Sep. 2013, Art. no. 104510. doi: 10.1103/PhysRevB.88.104510.

[22] D. Destraz, K. Ilin, M. Siegel, A. Schilling, and J. Chang, "Superconducting fluctuations in a thin NbN film probed by the Hall effect," *Phys. Rev. B, Condens. Matter*, vol. 95, no. 22, Jun. 2017, Art. no. 224501. doi: 10.1103/PhysRevB.95.224501.

[23] M. E. Cage and A. Jeffery, "A problem in ac quantized Hall resistance measurements and a proposed solution," *J. Res. Natl. Inst. Stand. Technol.*, vol. 103, no. 6, pp. 593–604, Nov./Dec. 1998. doi: 10.6028/jres.103.038.

[24] C.-C. Kalmbach *et al.*, "Towards a graphene-based quantum impedance standard," *Appl. Phys. Lett.*, vol. 105, no. 7, Aug. 2014, Art. no. 073511. doi: 10.1063/1.4893940.